All-Digital Blind Background Calibration Technique for Any Channel Time-Interleaved ADC

Yongtao Qiu, You-Jiang Liu, *Member, IEEE*, Jie Zhou, Guifu Zhang, Dahai Chen, and Niantong Du

***Abstract*— This paper proposes a novel digital adaptive blind background calibration technique for the gain, timing skew, and offset mismatch errors in a time-interleaved analog-to-digital converter (TI-ADC). Based on the frequency-shifted basis functions generated only from the measured TI-ADC output, the three mismatch errors can be represented, extracted, and then subtracted from the TI-ADC output adaptively, which is quite different from the conventional methods (e.g., using a bank of adaptive FIR filters). The advantage of the proposed technique is that it only needs to know the measured output signal and the TI-ADC channel number, without needing any additional information; and it is applicable to any TI-ADCs with no limitations to the channel number, sub-ADC sampling rate, signal type, and so on. Specifically, the frequency-shifted signal generator employs the Hilbert transform and does not need extra finite impulse response filters. Extensive simulation and measurement results have been presented to demonstrate the effectiveness and superiority of the proposed technique, for single-tone, multi-tone, wideband modulated, and multi-band modulated signals. In the measurement for a 32GS/s 16-channel TI-ADC system, it shows that the proposed technique can improve the effective number of bit by 2 ∼ 3 bit and the SFDR by 30 ∼ 35 dB.**

***Index Terms*— Time-interleaved analog-to-digital converter (TI-ADC), Hilbert transform, timing skew, blind calibration, effective number of bit (ENOB).**

I. Introduction

A TIME-INTERLEAVED analog-to-digital converter (TI-ADC), which is widely used in high speed data communication systems, instrumentation and measurement systems, and other electronic circuits and systems, is a structure employing multiple sub-ADCs that cyclically sample the analog signal in parallel at different time instances [1]. These application systems have an increasing need for high speed analog-to- -digital conversion at reasonable power consumption without performance degradation, which brings a lot of difficulties to analog circuit designers [2]–[4].

Manuscript received August 15, 2017; revised October 28, 2017 and December 9, 2017; accepted January 2, 2018. This work was supported in part by the NSFC under Grant 61601425. This paper was recommended by Associate Editor A. M. A. Ali. *(Corresponding author: You-Jiang Liu.)*

Y. Qiu is with the Department of Engineering Physics, Tsinghua University, Beijing 100084, China, and also with the Institute of Electronic Engineering, China Academy of Engineering Physics, Mianyang 621900, China (e-mail: qiuyt685@163.com).

Y.-J. Liu is with the Institute of Electronic Engineering, China Academy of Engineering Physics, Mianyang 621900, China (e-mail: liuyj04@163.com).

J. Zhou, G. Zhang, D. Chen, and N. Du are with the Institute of Electronic Engineering, China Academy of Engineering Physics, Mianyang 621900, China.

Color versions of one or more of the figures in this paper are available online at http://ieeexplore.ieee.org.

Digital Object Identifier 10.1109/TCSI.2018.2794529

The performance of a monolithic ADC with any given technology is limited in the comparator's regeneration time and amplifier's settling time [4]. Moreover, the nonlinearity of the amplifier and comparator will become more significant as the power consumption increases. The TI-ADC architecture was proposed to alleviate these problems, which could achieve a higher sampling rate than any other ADC architectures [2]–[6]. It is noticed that there are still some circuit design challenges for TI-ADC system, such as multi-phase clock generation and ADC clock distribution networks [2], [4], [7]. However, the main drawback of the TI-ADC architecture is the analog component mismatches among the parallel sub-ADC channels, which cause the sampled signal in each sub-ADC to experience a different gain, timing skew and channel offset [6], [8]. Hence, the key to a high performance solution is to eliminate the mismatches among the sub-ADCs.

The common method to increase the effective resolution of a TI-ADC system can be implemented through mismatch calibration [9]. There have been numerous calibration techniques proposed in previous literatures for the TI-ADCs. Analog and mixed signal calibration techniques [10]–[12] have been proposed to calibrate a delay of a clock path by adjusting the capacitance of varactors, which are attached to the outputs of clock buffers. An important advantage of these techniques is the simplicity of hardware elements. However, they show limited effective performances of the TI-ADCs due to the circuit process, supply voltage, temperature variations and the thermal noise effects [13]. In comparison, the all-digital calibration techniques process the sample value in digital domain, which could avoid the drawbacks of analog circuits. Another advantage is the circuit area reduction in an advanced process technology associated with the digital techniques. Also these techniques can be easily transplanted into another TI-ADC system only by resetting some parameters.

The all-digital calibration of the TI-ADC mismatches has attracted much attention during the past decade [14]. The main focus has been on the calibration of gain [15]–[24] and timing skew [25]–[33]. These techniques can be divided into the non-blind and the blind ones. The non-blind techniques normally require a known signal to calculate the mismatch parameters or the filter coefficients [17], [18]. However, the parameters and coefficients must be recalculated when the magnitude of error changes, which makes it hard to satisfy a dynamic situation. Instead, the blind techniques [24], [25], [31]–[33] only require the number of channel and do not need any information of the sampled signal.

As all-digital blind calibration techniques do, the calibration model includes two important blocks, a mismatch parameter

estimation block and a correction block. Conventionally, a bank of adaptive filters are employed in the mismatch correction block [19]–[23], where the timing skew mismatches are corrected by adjusting the filter coefficients. However, the filter coefficients have to be calculated or stored in a look-up table (LUT) in advance, which increases the complexity of circuits design in the TI-ADC system. A calibration technique using only one FIR filter with fixed coefficients for the gain and timing skew mismatch is presented in [24]. In that work, the Hadamard transform is applied to modulate the output signal to generate pseudo aliasing signals, which saves a lot of effort for filter design. However, this technique needs to eliminate DC offset in advance. In addition, it limits its application to the TI-ADC with specific channel numbers, to ensure there are Hadamard transforms for the given channel number, e.g., 2, 4, 8, etc. Another digital calibration technique for timing skew is proposed in [25], where polyphase filters are applied to estimate the timing skew of each channel, making the calibration to operate at a low rate. However, all the channels must be calibrated at the same time, which means each channel must equip its own adaptive stochastic gradient descent (SGD) feedback. As the number of channels increases, the complexity and power consumption will be intolerable. In addition, this technique cannot deal with the offset and gain mismatches.

To avoid the above limitations in the existing techniques, this paper proposes an all-digital blind calibration technique for the TI-ADC, only needing to know the channel number and the sampled data. In comparison with the conventional techniques, it does not require a pilot input and additional reference channel. The adaptive filter banks used in the conventional methods are also eliminated. Instead, a Hilbert finite impulse response (FIR) filter is used to generate the basis functions to represent the spurious signals. Based on which, the gain, timing skew and offset mismatches can be estimated and cancelled from the generated frequency-shifted basis signals adaptively. At the top level, the proposed technique includes three blocks: the frequency shifting and folding (FSF) block, the coefficient estimation (CE) block and the offset generation (OG) block. The main advantage of the proposed all-digital blind technique is that it is applicable to any TI-ADCs with no limitation to the channel number and mismatch type. It is also effective to the TI-ADC sampling of single-tone, multi-tone, wideband modulated, and multi-band modulated signals. The remainder of this paper is organized as follows. In Section II, the mechanism of the spurious signals' generation in the TI-ADC system is reviewed. The proposed calibration technique using the frequency-shifted basis signals is presented in Section III. Extensive simulations are given in Section IV and experimental results are given in Section V. Finally, Section VI concludes this paper.

II. Spurious Signals Due to Gain and Timing Skew Mismatches

In this section we will introduce the system model of an M-channel TI-ADC, to analyze the spurious signals due to offset, gain and timing skew mismatches, based on which, the all-digital blind calibration scheme will be established in the upcoming section.

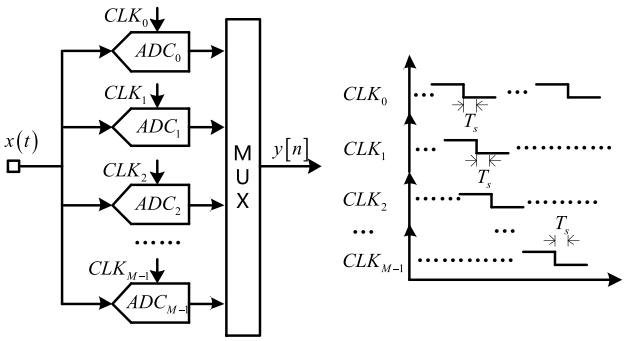

Fig. 1. M-channel TI-ADC and its timing diagram.

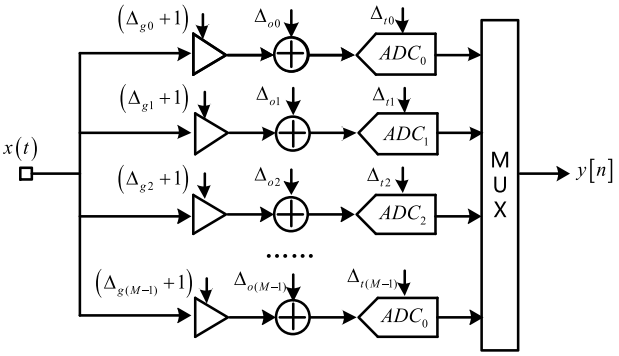

Fig. 2. M-channel TI-ADC with offset, gain and timing skew mismatches.

A block diagram and a timing diagram of the M-channel TI-ADC are shown in Fig. 1. Each channel consists of a sub-ADC, whose sampling period is MT_S. Then, the digital streams from the M channels are multiplexed to generate the ultimate ADC digital output with the sampling period of T_S. For an ideal TI-ADC, the output of the k-th channel is

$$y_k[n] = x[nM + k], \quad k = 0, 1, \ldots M-1 \tag{1}$$

Then the total output of the TI-ADC becomes

$$y[n] = y_k\left[\frac{n-k}{M}\right], \quad \text{where } k = n \bmod M \tag{2}$$

Actually, there are several sources of mismatches in the signal data path, which degrade the TI-ADC performances [5]. Each sub-ADC has its own gain $(1+\Delta_{gk})$, offset Δ_{ok}, and timing skew Δ_{tk}. Fig. 2 presents a block diagram of M-channel TI-ADC with these mismatches. The k-th channel transfer function can be written as [14]

$$H_k(j\omega) = (1+\Delta_{gk})\, e^{j\omega(k+\Delta_{tk})}, \quad k = 0,\ 1, \ldots M-1 \tag{3}$$

Thus, the DFT of the down-sampled signal by excluding the offset in the k-th channel can be written as [24]

$$Y_k(j\omega) = e^{-jk\omega}\frac{1}{M}\sum_{i=0}^{M-1}\left[H_k\left(j\left(\omega - 2\pi i/M\right)\right) \times X\left(j\left(\omega - 2\pi i/M\right)\right)\right] \tag{4}$$

where $X(j\omega)$ is the DFT of the ideal reference input signal $x[n]$. Noticing that the offset mismatch is independent of input signal, it can be directly added to the (4). Therefore, the DFT of the reconstructed TI-ADC real-valued output signal $y[n]$ can be expressed as

$$\begin{aligned} Y(j\omega) &= \sum_{k=0}^{M-1} Y_k(j\omega) + \sum_{k=0}^{M-1} O_k(j\omega) \\ &= \hat{X}(j\omega) + \sum_{i=1}^{M-1} S_i(j\omega) + \sum_{k=0}^{M-1} O_k(j\omega) \end{aligned} \quad (5)$$

with

$$\begin{aligned} \hat{X}(j\omega) &= \left[\frac{1}{M}\sum_{k=0}^{M-1}\left(1+\Delta_{gk}\right)e^{j\omega\Delta_{tk}}\right] \times X(j\omega) \\ S_i(j\omega) &= \left[\frac{1}{M}\sum_{k=0}^{M-1}\left(1+\Delta_{gk}\right)e^{-2\pi ikj/M}e^{j(\omega-2\pi i/M)\Delta_{tk}}\right] \\ &\quad \times X\left(j\left(\omega-2\pi i/M\right)\right) \end{aligned} \quad (6)$$

where $\hat{X}(j\omega)$ represents the desired signal, which is the amplitude modulated copy of ideal input signal. $O_k(j\omega)$ is the spur due to offset, which is amplitude modulated single tone. $S_i(j\omega)$ is the spurious signal due to gain and timing skew, which is generated from the amplitude modulated and frequency shifted copy of the ideal input signal. For an ideal TI-ADC, gain and timing skew in each sub-ADC is identical, thus the spurious signals will be perfectly canceled. In practice, each channel experiences a different gain, timing skew and channel offset, which significantly reduce the performance measures such as the signal-to-noise and distortion ratio (SNDR) and the spurious-free dynamic range (SFDR) [26]–[29]. Taking a 4-channel TI-ADC for instance, the spectrum of the real-valued output signal is shown in Fig. 3. It is noticed that the spurious signals due to gain and timing skew own the similar expression as the desired signal. Specifically, $S_i(j\omega)$ can be represented by $\hat{X}(j\omega)$ after frequency shifting and folding, which is the core idea of the proposed technique. In addition, the spurs due to offset are spaced at $2\pi k/M$, which can be modeled as δ-function. The specific analysis is presented in the next section.

III. Proposed All-Digital Blind Calibration Technique

In this section, an adaptive blind calibration technique is pr-oposed to calibrate the mismatches in M-channel TI-ADC. Firstly, the theoretical model of M-channel TI-ADC is developed based on the basis functions of the spurious signals. Then utilizing this model, the mismatch calibration structure is presented.

A. Model of M-Channel TI-ADC

As it is mentioned in section II, the spurs due to offset can be represented by a group of δ- functions, that is

$$O_{B,k}(j\omega) = \delta\left(j\left(\omega - 2k\pi/M\right)\right), \quad (k = 0, 1, \ldots, M-1) \quad (7)$$

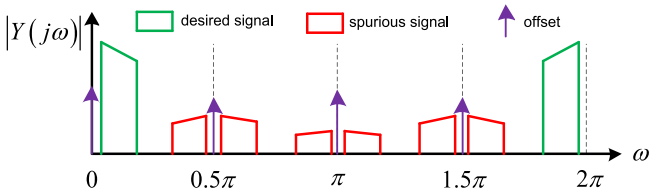

Fig. 3. The output spectrum of a 4-channel TI-ADC.

Similarly, the spurious signals due to gain and timing skew have the basis functions in the form of

$$S_{B,i}(j\omega) = \hat{X}\left(j\left(\omega - 2\pi i/M\right)\right), \quad (i = 1, \ldots, M-1) \quad (8)$$

Thus the frequency domain of the M-channel TI-ADC output could be modified as follows

$$Y(j\omega) = \hat{X}(j\omega) + \sum_{i=1}^{M-1} w_{s,i} S_{B,i}(j\omega) + \sum_{k=0}^{M-1} w_{o,k} O_{B,k}(j\omega) \quad (9)$$

with

$$\begin{aligned} S_i(j\omega) &= w_{s,i} S_{B,i}(j\omega), \quad i = 1, \ldots, M-1 \\ O_k(j\omega) &= w_{o,k} O_{B,k}(j\omega), \quad k = 0, 1, \ldots, M-1 \end{aligned} \quad (10)$$

where $w_{s,i}$ and $w_{o,k}$ donate the mismatch coefficients of gain/timing skew and offset respectively. In the conventional calibration methods [14], [24], [25], the desired signal $\hat{X}(j\omega)$ is generally regard as the ideal input signal $X(j\omega)$. Since the mismatch coefficient of gain/timing skew is a function of $j\omega$, thus the derivative filters are required to generate the basis functions in the conventional calibration structures. Actually, the desired signal consists of both linear component and derivative component, which can be utilized to generate the basis functions for gain/timing skew mismatches directly. In addition, the coefficients of offset are M fixed constants independent of input signal, which can be inferred from Fig. 3. Thus it is reasonable to choose the δ-function as the basis functions.

B. Real-Valued Basis Functions

It is noticed that the IDFT of (9) is complex-valued signal, which cannot be applied to the real-valued signal directly. Considering that the frequency spectrum of the desired signal (real-valued) is symmetric around the y axis (positive frequency part and negative frequency part), Hilbert transform (HT) is applied in the calibration technique to generate the basis functions. In this subsection, detailed analysis is presented to illustrate the implementation of basis-function generation.

1) Basis Functions of Gain and Timing Skew: First, the complex -valued signal is generated from the desired signal $\hat{x}[n]$, e.g., via Hilbert transform (HT) as

$$\hat{x}_c[n] = \hat{x}[n] + j\left\{\hat{x}[n] * h_{HT}[n]\right\} \quad (11)$$

where $h_{HT}[n]$ denotes the impulse response of Hilbert filter and the $*$ means convolution operation. Then, the frequency

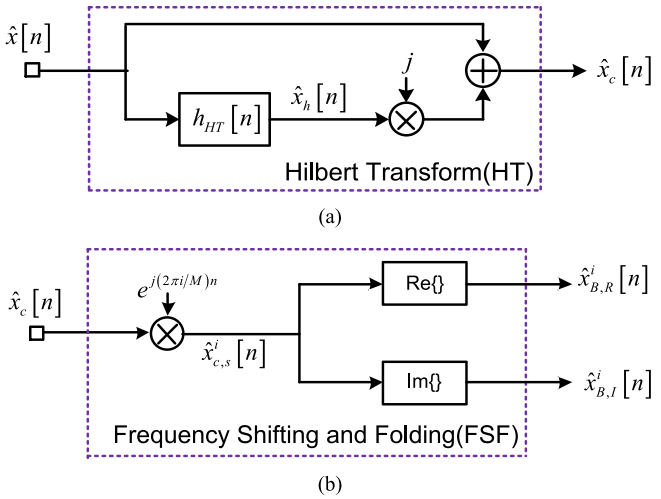

Fig. 4. Diagram of (a) Hilbert Transform and (b) Frequency Shifting and Folding.

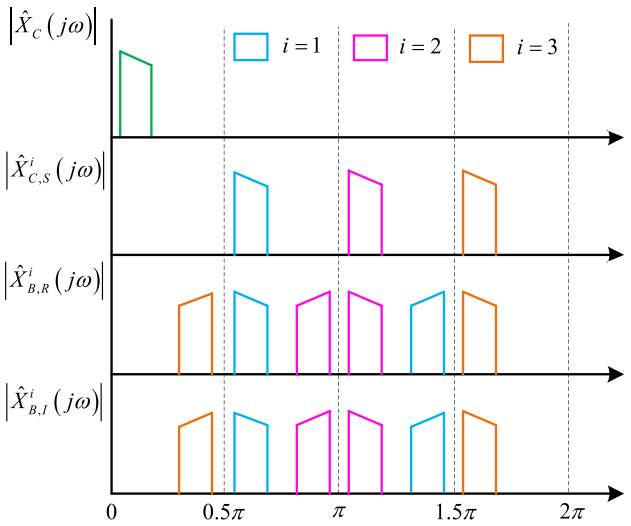

Fig. 5. The spectrum of $\hat{x}_c[n]$, $\hat{x}^i_{c,s}[n]$, $\hat{x}^i_{B,R}[n]$and $\hat{x}^i_{B,I}[n]$ in a 4-channel TI-ADC.

shifting operation could be implemented as follows

$$\hat{x}^i_{c,s}[n] = \hat{x}_c[n] \cdot \exp[j(2\pi i/M)n], \quad i = 1, 2, \ldots, M-1 \tag{12}$$

Since the real-valued signal consists of image components in frequency domain around π (see Fig. 5 later), the frequency folding operation is required as follows

$$\begin{aligned} \hat{x}^i_{B,R}[n] &= Re\left\{\hat{x}^i_{c,s}[n]\right\} \\ \hat{x}^i_{B,I}[n] &= Im\left\{\hat{x}^i_{c,s}[n]\right\} \end{aligned} \tag{13}$$

where $Re\{\cdot\}$ and $Im\{\cdot\}$ indicate the real part and the imaginary part of a complex number respectively. The real valued signal $\hat{x}^i_{B,R}[n]$ and $\hat{x}^i_{B,I}[n]$ are the basis functions of gain and timing skew. The whole basis-function generation flow is depicted in Fig. 4. Furthermore, the spectrums of$\hat{x}_c[n]$, $\hat{x}^i_{c,s}[n]$, $\hat{x}^i_{B,R}[n]$ and $\hat{x}^i_{B,I}[n]$ in a 4-channel TI-ADC are displayed in Fig. 5 to illustrate the generation process of basis functions. It should be noticed that the basis function $\hat{x}^i_{B,R}[n]$

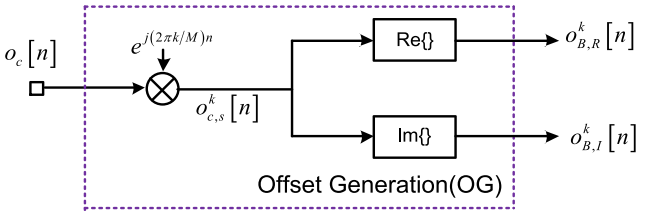

Fig. 6. Diagram of offset generation.

and $\hat{x}^i_{B,I}[n]$ contain different frequency information although their spectrums are in the same shape.

2) Basis Functions of Offset: the analysis of offset in the above section indicates that we can choose a function as follows

$$o_c[n] = e^{j2\pi n} \tag{14}$$

Similarly, the frequency shifting operation is given by

$$o^k_{c,s}[n] = o_c[n] \cdot \exp[j(2\pi k\ M)n], \quad k = 0, 1, \ldots, M-1 \tag{15}$$

This leads to the basis functions of the form

$$\begin{aligned} o^k_{B,R}[n] &= Re\left\{o^k_{c,s}[n]\right\} \\ o^k_{B,I}[n] &= Im\left\{o^k_{c,s}[n]\right\} \end{aligned} \tag{16}$$

Stemming from Fig. 4(b), the generation of the above basis functions can be accomplished in the similar manner by replacing $\hat{x}_c[n]$ with $o_c[n]$ as depicted in Fig. 6. Therefore, the output signal can be reconstructed by the proposed basis functions

$$\begin{aligned} y[n] = \hat{x}[n] + \underbrace{\sum_{i=1}^{M-1}\left(c^i_{B,R}\hat{x}^i_{B,R}[n] + c^i_{B,I}\hat{x}^i_{B,I}[n]\right)}_{\text{spurious signals due to gain and timing skew}} \\ + \underbrace{\sum_{k=0}^{M-1}\left(c^k_{O,R}o^k_{B,R}[n] + c^k_{O,I}o^k_{B,I}[n]\right)}_{\text{spurs due to offset}} \end{aligned} \tag{17}$$

where $c^i_{B,R}$ and $c^i_{B,I}$ are the coefficients of gain and timing skew mismatch. $c^k_{O,R}$ and $c^k_{O,I}$ are the coefficients of offset mismatch. It is noticed that (17) is the real-valued form of the M-channel TI-ADC, which can be used to calibrate the mismatches directly. The calibration structure is introduced in the next subsection.

C. Calibration Structure

The basis function generation method in the prior analysis is based on the assumption that the desired signal $\hat{x}[n]$ is already known. Actually in a blind calibration structure, the only information can be obtained are the output signal $y[n]$ and the channel number M. Considering that the power of spurious signals is normally much lower than that of the desired signal, an initialized approximation is given as

$$\hat{x}[n] \rightarrow^{\text{Replaced by}} y[n] \tag{18}$$

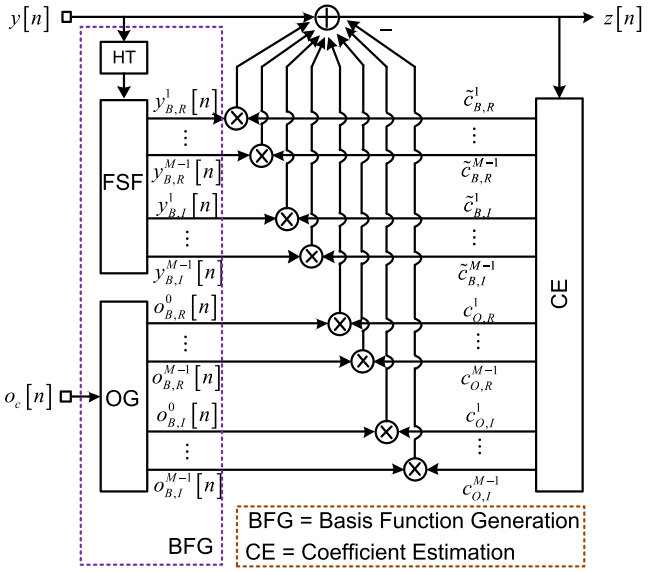

Fig. 7. Diagram of the proposed calibration structure.

for the basis functions generation in (13). By feeding $y[n]$ into the Hilbert Transform (HT) block and then the Frequency Shifting and Folding (FSF) block, as illustrated in Fig. 4, it yields a group of new basis functions $y^i_{B,R}[n]$ and $y^i_{B,I}[n]$. The basis functions of offset is still generated as depicted in Fig.6 since the offset mismatch is independent of the input signal. Since the basis functions own the same frequency components as the spurious signals, thus the spurious signals can be cancelled via subtracting the basis functions weighted by a group of suitable coefficients.

A block diagram of the proposed calibration structure is depicted in Fig.7. The FSF block and OG block are applied to generate the basis functions to cancel the spurious signals, which are combined as the BFG block for simplicity. The mismatch coefficients are extracted from CE block. Then the calibrated signal is written as

$$\begin{aligned} z[n] &= y[n] - \tilde{e}[n] \\ &= y[n] - \sum_{i=1}^{M-1}\left(\tilde{c}^i_{B,R} y^i_{B,R}[n] + \tilde{c}^i_{B,I} y^i_{B,I}[n]\right) \\ &\quad - \sum_{k=0}^{M-1}\left(c^k_{O,R} o^k_{B,R}[n] + c^k_{O,I} o^k_{B,I}[n]\right) \end{aligned} \tag{19}$$

where $\tilde{c}^i_{B,R}$ and $\tilde{c}^i_{B,I}$ are the estimation of $c^i_{B,R}$ and $c^i_{B,I}$ in (17). The coefficient estimation will be introduced in the next subsection.

D. Coefficient Estimation

In the coefficient estimation structure, the BFG block is also applied to generate the basis functions as depicted in Fig. 8. In order to estimate the coefficients adaptively, a method based on least mean squares (LMS) algorithm is proposed. For simplicity, the estimation of spurious signals from the n-th calibrated sample $z[n]$ of the CE block can be rewritten in

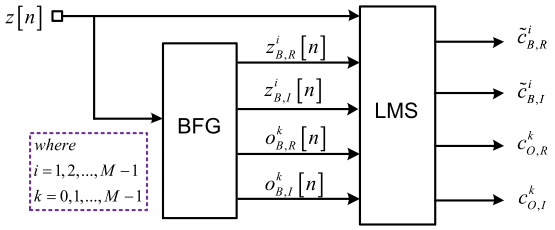

Fig. 8. Diagram of the coefficient estimation (CE) structure.

matrix form

$$\tilde{e}_{CE}[n] = \tilde{\mathbf{c}}_{\mathbf{B,R}}\mathbf{z}_{\mathbf{B,R}} + \tilde{\mathbf{c}}_{\mathbf{B,I}}\mathbf{z}_{\mathbf{B,I}} + \mathbf{c}_{\mathbf{O,R}}\mathbf{o}_{\mathbf{B,R}} + \mathbf{c}_{\mathbf{O,I}}\mathbf{o}_{\mathbf{B,I}} \tag{20}$$

where

$$\begin{aligned} \tilde{\mathbf{c}}_{\mathbf{B,R}} &= \left[c^1_{B,R}, c^2_{B,R}, \ldots, c^{M-1}_{B,R}\right] \\ \tilde{\mathbf{c}}_{\mathbf{B,I}} &= \left[c^1_{B,I}, c^2_{B,I}, \ldots, c^{M-1}_{B,I}\right] \\ \mathbf{c}_{\mathbf{O,R}} &= \left[c^0_{O,R}, c^1_{O,R}, \ldots, c^{M-1}_{O,R}\right] \\ \mathbf{c}_{\mathbf{O,I}} &= \left[c^0_{O,I}, c^1_{O,I}, \ldots, c^{M-1}_{O,I}\right] \\ \mathbf{z}_{\mathbf{B,R}} &= \left[z^1_{B,R}[n]; z^2_{B,R}[n]; \ldots; z^{M-1}_{B,R}[n]\right] \\ \mathbf{z}_{\mathbf{B,I}} &= \left[z^1_{B,I}[n]; z^2_{B,I}[n]; \ldots; z^{M-1}_{B,I}[n]\right] \\ \mathbf{o}_{\mathbf{B,R}} &= \left[o^0_{B,R}[n]; o^1_{B,R}[n]; \ldots; o^{M-1}_{B,R}[n]\right] \\ \mathbf{o}_{\mathbf{B,I}} &= \left[o^0_{B,R}[n]; o^1_{B,R}[n]; \ldots; o^{M-1}_{B,R}[n]\right] \end{aligned} \tag{21}$$

The estimation error can be expressed as

$$\varepsilon[n] = e_{CE}[n] - \tilde{e}_{CE}[n] = \left(z[n] - \hat{x}[n]\right) - \tilde{e}_{CE}[n] \tag{22}$$

With the cost function (22), the mismatch coefficients can be estimated by finding the minimum of $\varepsilon^2[n]$ exploiting the iteration equation as

$$\begin{aligned} \tilde{c}^i_{B,R}[n+1] &= \tilde{c}^i_{B,R}[n] + \mu_{B,R}\left(z[n] z^i_{B,R}[n]\right) \\ \tilde{c}^i_{B,I}[n+1] &= \tilde{c}^i_{B,I}[n] + \mu_{B,I}\left(z[n] z^i_{B,I}[n]\right) \\ c^k_{O,R}[n+1] &= c^k_{O,R}[n] + \mu_{O,R}\left(z[n] o^k_{B,R}[n]\right) \\ c^k_{O,I}[n+1] &= c^k_{O,I}[n] + \mu_{O,I}\left(z[n] o^k_{B,I}[n]\right) \\ & \qquad i = 1, 2, \ldots, M-1 \quad \text{and } k = 0, 1, \ldots, M-1 \end{aligned} \tag{23}$$

where $\mu_{B,R}$, $\mu_{B,I}$, $\mu_{O,R}$ and $\mu_{O,I}$ are the adaptation step of $\tilde{c}^i_{B,R}$, $\tilde{c}^i_{B,I}$, $c^k_{O,R}$ and $c^k_{O,I}$ respectively. Actually, the iteration of mismatch coefficients is based on the correlation of $z[n]$ and the basis functions. When the spurious signals decrease, a feedback makes the correlation value converge to zero. Compared with [24], the proposed calibration method could compensate the offset, gain and timing skew mismatch in one structure without using any DC canceller in advance.

The key idea of the proposed method is to construct the basis functions to represent the spurious signals. The basis functions are generated from the sampled signal $y[n]$ by using HT and FSF block as in Fig. 4. In addition, the LMS

algorithm is applied to estimate the mismatch coefficients. This makes the proposed method to be an adaptive blind calibration technique. It should be noticed that there are still some limitations similar to the conventional methods. As depicted in Fig. 5, the basis function will overlap with the desired signal when the input signal is single-tone spaced at $k\pi/M$. Thus, the frequency of a single-tone input should avoid$k\pi/M$. But there is no such limitation when the input is a wideband signal.

IV. Simulation Results

In this section, the simulation results for the proposed blind calibration structure are presented. The overall performance of the blind calibration structure was evaluated by signal-to-noise ratio (SNR) and spurious free dynamic range (SFDR). The SNR before calibration was written as [31]

$$SNR = 10\log_{10}\frac{\sum_{n=1}^{N}|x[n]|^2}{\sum_{n=1}^{N}|x[n]-y[n]|^2} \tag{24}$$

and after calibration as

$$SNR = 10\log_{10}\frac{\sum_{n=1}^{N}|x[n]|^2}{\sum_{n=1}^{N}|x[n]-z[n]|^2} \tag{25}$$

where N is the length of samples used to calculated the SNR. The proposed calibration method was simulated for a 4-channel TI-ADC and 16-channel TI-ADC respectively.

A. Implementation of the Basis Function Generation

In the blind calibration structure, the Hilbert transform was implemented through a fixed FIR filter. The taps of the filter $h[n]$ was 31, and it was designed using MATLAB function "firpm". By replacing $\hat{x}[n]$ with $y[n]$ in Fig. 4, the basis functions of gain and timing skew can be simplified as

$$\begin{bmatrix} y^i_{B,R}[n] \\ y^i_{B,I}[n] \end{bmatrix} = \begin{bmatrix} \cos\dfrac{2\pi ni}{M} & -\sin\dfrac{2\pi ni}{M} \\ \sin\dfrac{2\pi ni}{M} & \cos\dfrac{2\pi ni}{M} \end{bmatrix} \begin{bmatrix} y[n-K] \\ y_h[n] \end{bmatrix} \tag{26}$$

with

$$y_h[n] = y[n] * h[n] \tag{27}$$

where K is the delay of the linear-phase Hilbert filter $h[n]$. The implementation architecture of basis function generation is depicted in Fig. 9. Similarly, the basis functions of offset can be rewritten as

$$\begin{aligned} o^k_{B,R}[n] &= \cos(2\pi kn/M) \\ o^k_{B,I}[n] &= \sin(2\pi kn/M) \end{aligned} \tag{28}$$

In practice, the generation of basis functions and estimation of mismatch coefficients only require addition and multiplication operations. Specifically, LMS algorithm is applied to calibrate the mismatches sample by sample, which could adapt to an online TI-ADC system.

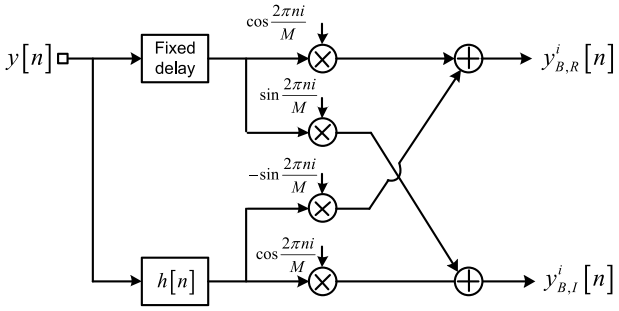

Fig. 9. Implementation architecture of the basis function generation.

TABLE I
Added Coefficients of Mismatches in The 4-Channel TI-ADC

Channel	0	1	2	3
Offset (A)	0.04	-0.05	-0.06	0.06
Gain	1.06	1.08	0.95	0.93
Timing skew (Ts)	0.01	-0.01	0.008	-0.015

B. Simulations of 4-Channel TI-ADC

In this subsection, the calibration of a 4-channel TI-ADC with offset, gain and timing skew mismatches is presented. The quantization error is usually very small in the TI-ADC system. If the mismatch errors are as small as the quantization error, the overall ADC can be considered almost ideal [27]. Thus, the quantization noise was negligible in the simulations the same as [24], [25], and [27]. The simulated TI-ADC model is given in Fig. 2. The coefficients of offset, gain and timing skew are shown in Table I.A is the amplitude of the input signal and T_s is the sample period of TI-ADC. The number of samples was 2^{16} and all the adaption steps were chosen as 2^{-13} to make a tradeoff between the speed of convergence and the stability of the coefficients. In the proposed technique, the adaptation step below 2^{-11} could guarantee the stability of the coefficients. It should be noticed that the choice of adaptation step in the blind LMS algorithm is usually based on the simulation results, such as [24], [25], and [32]. When we focus on the convergence speed, we should choose a larger adaptation step. When we demand an excellent SNDR performance, a smaller adaptation step would be a nice choice.

Fig.10 (a) shows the spectrum of the uncalibrated 4-channel TI-ADC output and the calibrated signal. The SNR and SFDR before calibration are 19.52 dB and 21.69 dB respectively, while after calibration the SNR and SFDR are 56.07 dB and 65.41 dB. The corresponding convergence curves of coefficients are presented in Fig.10 (b). The mismatch coefficients begin to converge when the number of sample reaches 4×10^4. Actually, the proposed method only requires that the power of the desired signal is higher than the spurious signals. Even when the spurs are close to the desired signal, the proposed method is still effective as shown in Fig. 10 (c). Further, the multi-tone and 16QAM input were fed to the TI-ADC system respectively. Fig. 11 presents the spectrum of the

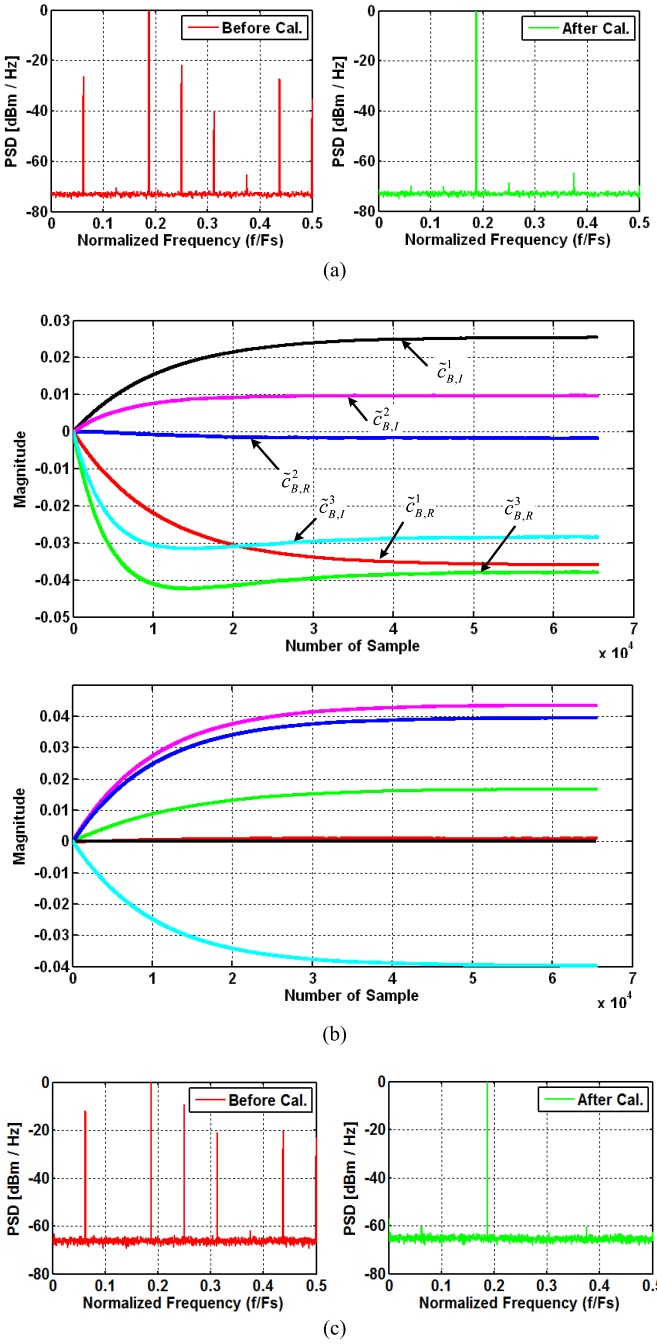

Fig. 10. Simulation of 4-channel TI-ADC (a) the spectrum of the uncalibrated and calibrated signal, (b) the convergence curves of coefficients and (c) the calibration of the input signal with high power spurs.

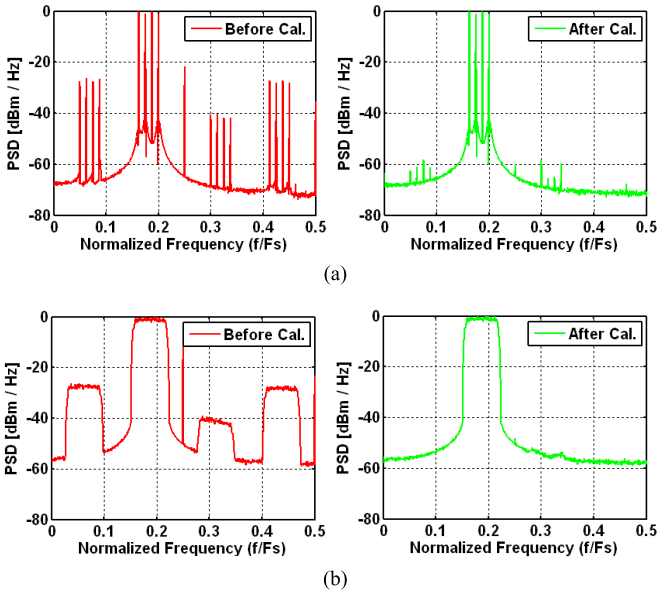

Fig. 11. Spectrum of 4-channel TI-ADC before/after calibration when input signal is (a) multi-tone and (b) 16QAM.

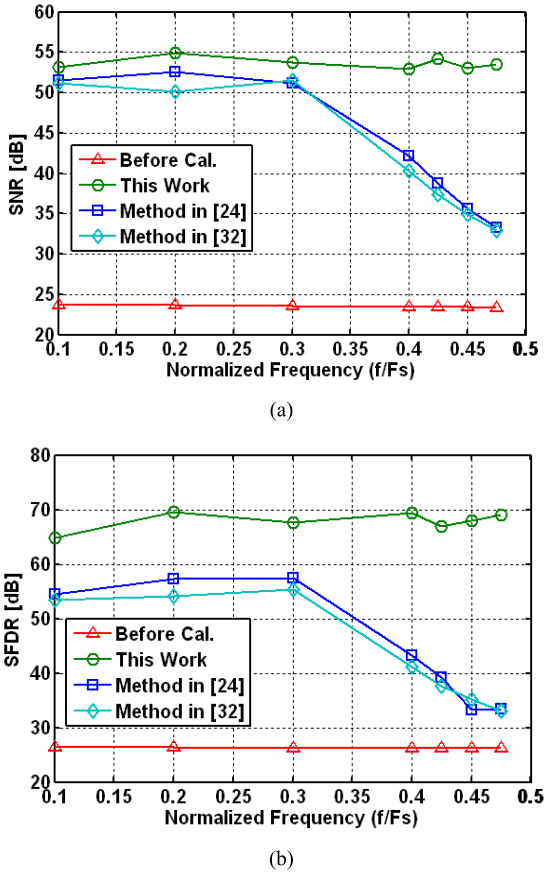

Fig. 12. SNR/SFDR performances versus input frequency (a) SNR , (b)SFDR.

uncalibrated output and calibrated output. The SNR before calibration were 22.17 dB and 22.24 dB respectively, and after calibration the SNR were 56.25 dB and 56.31 dB respectively. In summary, the proposed calibration technique could adapt to single-tone, multi-tone and 16QAM input. In addition, the offset, gain and timing skew mismatch could be compensated simultaneously based on the proposed calibration structure.

Then we compared the SNR and SFDR performances with the conventional calibration method in [24] and [32] by utilizing a single-tone input whose frequency varies from 0 to Fs/2. Since the calibration methods proposed in [24] and [32] are incapable of handling the offset mismatch, the coefficients of offset were set as zero in this simulation. Fig.12 depicts the

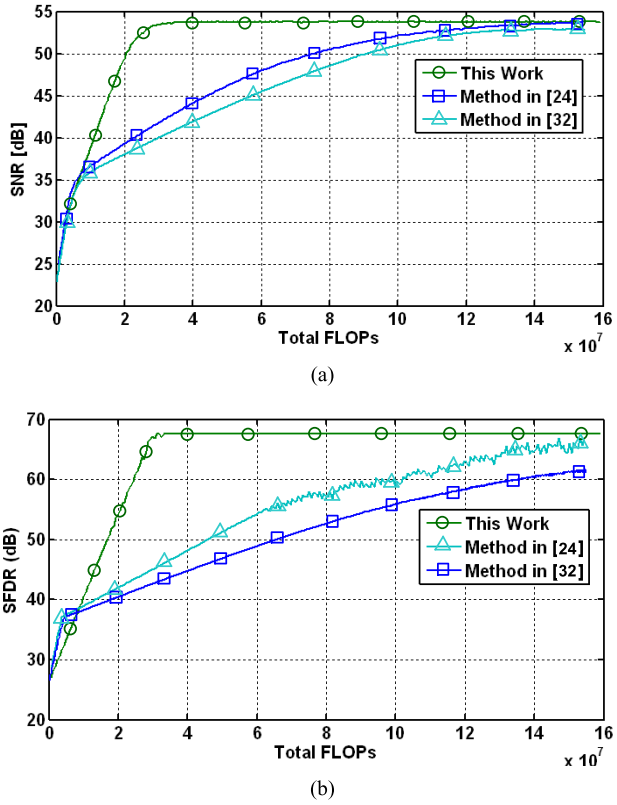

Fig. 13. SNR/SFDR performances versus the total FLOPs (a) SNR, (b) SFDR.

SNR and SFDR performances versus input frequency. The SNR and SFDR performances of the conventional methods significantly degrade at high-end frequencies. Instead, the proposed method can achieve an improvement of 30 dB for SNR and 40 dB for SFDR, which is effective in the whole Nyquist zone.

In addition, the computational complexity was simulated depending on the implementation of the calibration structure. Referring to the calibration structure mentioned before, the addition operation Ra and multiplication operation Rm in one calibration cycle can be expressed as

$$\begin{aligned} Ra &= (M-1)(2L+4)+L-1 \\ R &= (M-1)(2L+8)+L \end{aligned} \tag{29}$$

where L and M donates the length of Hilbert filter and the channel number respectively. According to the operation- -FLOP conversion in [34], the FLOPs used in one calibration cycle can be written as

$$\text{FLOPs} = (M-1)(4L+12)+2L-1 \tag{30}$$

We chose a fixed input frequency $f = 0.3Fs$ to compare the computational complexity with that of the conventional method in [24] and [32]. Similarly, the coefficients of offset were set as zero in this simulation. The simulations were implemented in the same condition to make a fair comparison. Fig.13 depicts the SNR and SFDR performances versus the total FLOPs respectively. Based on the proposed calibration structure, the SNR and SFDR converges when the total FLOPs reaches 4×10^7, which is much faster than the conventional methods in [24] and [32].

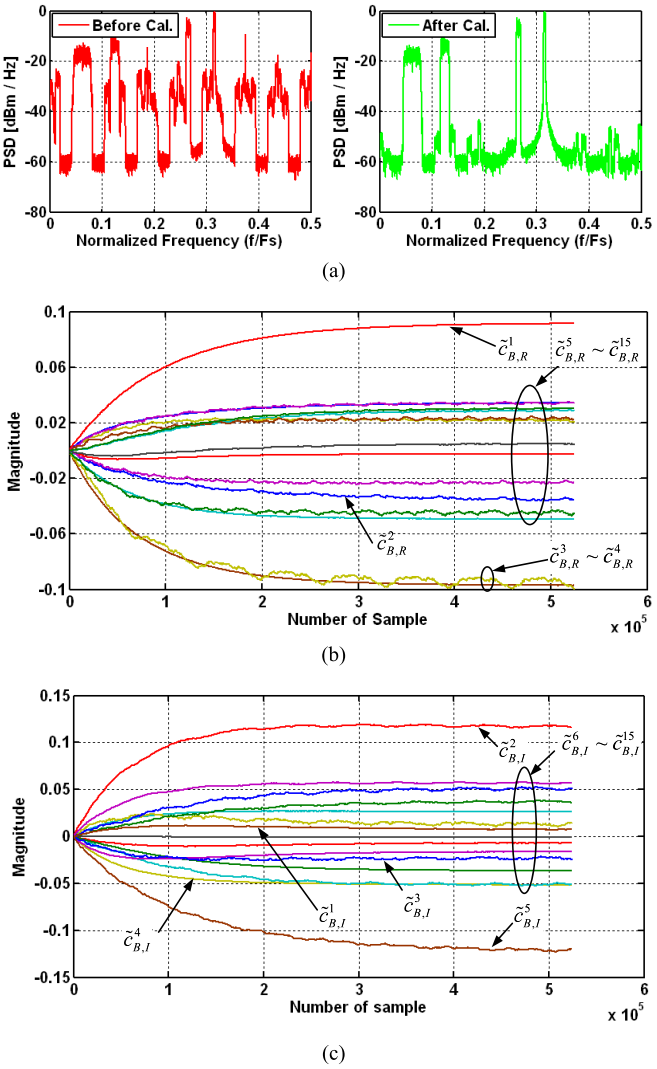

Fig. 14. (a) Spectrum of the 16-channel TI-ADC before/after calibration, (b) the convergence curves of coefficients $\tilde{c}^1_{B,R} \sim \tilde{c}^{15}_{B,R}$ and (c) the convergence curves of coefficients $\tilde{c}^1_{B,I} \sim \tilde{c}^{15}_{B,I}$.

C. Simulations of 16-Channel TI-ADC

The simulation of 16-channel TI-ADC is further presented in this subsection to demonstrate the effectiveness of the proposed method. A multi-band input was tested in the 16-channel TI-ADC, which was used to simulate the scenario of a multi-carrier digital communication signals. Similarly, the quantization noise was negligible. The number of samples was 2^{18} and the adaption steps were set as 2^{-16}. Fig.14 (a) presents the spectrum of the uncalibrated 16-channel TI-ADC output and the calibrated signal. The SNR and SFDR before calibration are 12.21 dB and 9.30 dB respectively, while after calibration the SNR and SFDR are 39.54 dB and 43.19 dB. The corresponding convergence curves of coefficients are depicted in Fig.14 (b) and Fig.14 (c), which indicates that the mismatch coefficients begin to converge when the number of sample reaches 4×10^5.

TABLE II
FPGA SYNTHESIS RESULTS

	[25]	[32]	This Work
Family	Stratix IV	Stratix IV	Kintex7
Device	EP4SGX230 KF40C2	EP4SGX230 KF40C2	7K325TFBG 900-2
Number of LUTs	8779/182400	4687/182400	4166 /203800
Number of Registers	7741	4183	1194
Number of DSP block	24/1288	24/1288	26/840
Adders	—	—	26
Multipliers	—	—	28
Fmax	194.29 MHz	186.95 MHz	221.27 MHz

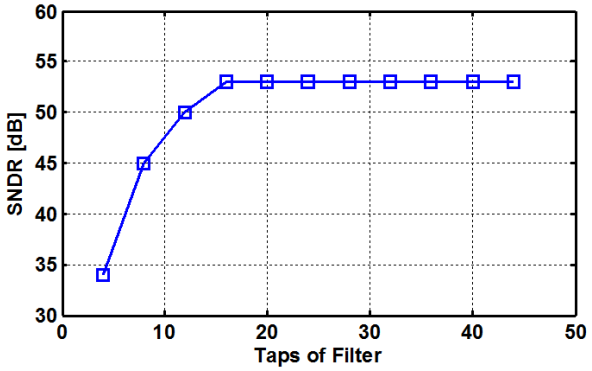

(a)

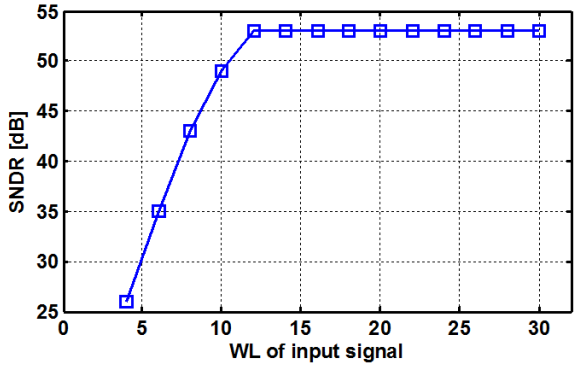

(b)

Fig. 15. SNDR performance versus (a) the taps of filter and (b) the wordlength of input signal.

D. Hardware Validation

The hardware implementation of the proposed calibration architecture was validated on the Xilinx FPGA board with the Kintex7 7k325tfbg900-2 chip. The calibration model and the test-bench environment are all implemented in ISE14.7 with VHDL language. The trigonometric functions in Fig. 9 were groups of fixed-value number with the period of M, which were set as several fixed signals in the VHDL implementation. As shown in Table II, the design can operate on the FPGA at the clock frequency of 221 MHz and consume very few percentage of hardware resources in the FPGA chip. In comparison with the two state-of-the-arts, the proposed technique requires less hardware resources and could reach a higher speed on FPGA. In addition, the SNDR performance versus the number of taps and the signal Word Length (WL) was investigated based on the binary representation in FPGA chip as shown in Fig. 15. The SNDR converges to a stable point when the taps of filter reaches 16 and the WL of the input signal reaches 12.

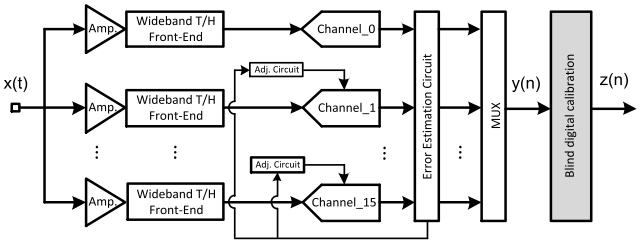

Fig. 16. The block diagram of the 32GS/s TI-ADC system.

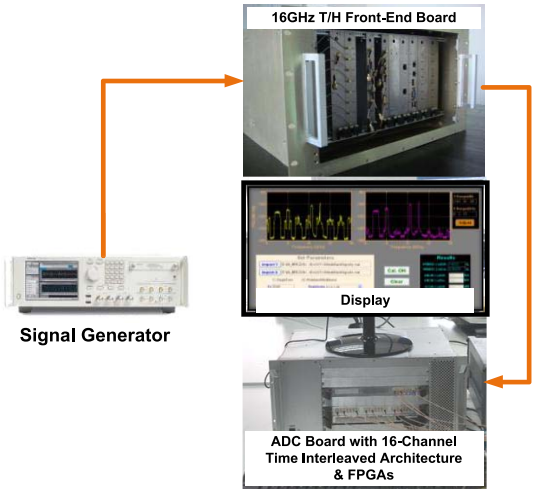

Fig. 17. Measured device of the TI-ADC system.

V. EXPERIMENTAL RESULTS

In this section, the performance of the proposed calibration technique was experimentally tested in a 32GS/s 16-channel TI-ADC system. As depicted in Fig. 16, the proposed 32GS/s TI-ADC system is composed of an ultra-wideband distributed amplification and T/H network, which could support up to 18 GHz 3-dB bandwidth, resulting in about 16 GHz available bandwidth for practical applications. The input analog signal is first divided into 16-channel and amplified by the high gain and low noise figure amplifiers respectively. Subsequently, the 16-channel signals are sampled by 16 sub-ADCs with clock rate of 2 GHz. In addition, an online estimation network is applied to extract the raw errors and then adjust the clock phase, channel gain and offset voltage, which can make sure the TI-ADC output to be reasonably reconstructed. However,

TABLE III
A BRIEF COMPARISON WITH THE STATE-OF-THE-ART TECHNIQUES

Characteristics	[17]	[24]	[25]	[32]	[33]	This work
Blind or Non-blind	Semi-blind	Blind	Blind	Blind	Blind	Blind
Requiring Additional Ref. Channel	No	No	No	No	Yes	No
M (#of Sub-ADC Channel)	2	Must have Hadamard matrix (e.g., 2,4,8,12…)	4	Must have Hadamard matrix (e.g., 2,4,8,12…)	2 / 4	Any
Signal Under Test	Wideband	Multi-tone	Multi-tone	Multi-tone	White Gaussian Noise	Single tone Multi-tone Wideband Multi-band
Mismatch Type	Gain Timing skew	Gain Timing skew	Timing skew	Gain Timing skew	Offset Gain Timing skew	Offset Gain Timing skew

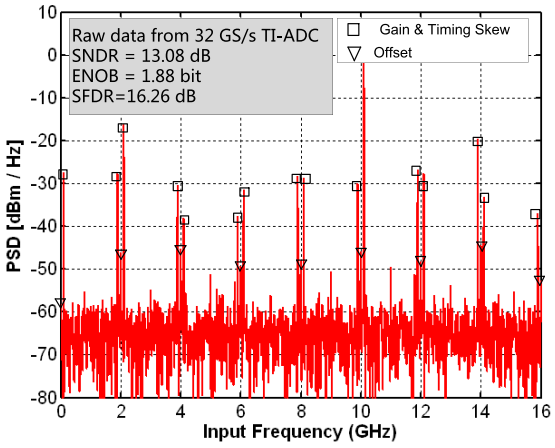

(a)

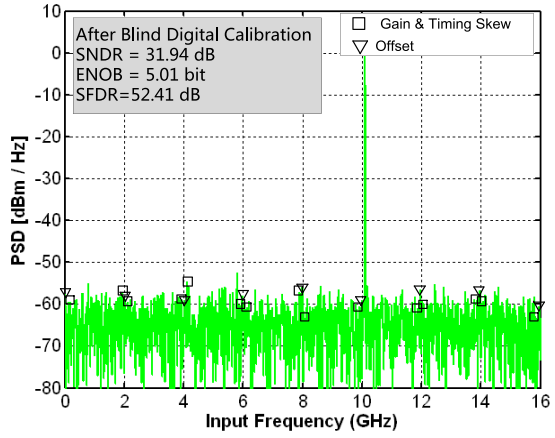

Fig. 18. Measured results of the TI-ADC for a single-tone (a) before calibration and (b) after calibration.

since the analog adjustment circuits cannot cover enough high bandwidth range and the accuracy of the circuits are limited to the phase noise of the clock, the online adjustment network is not able to provide enough accuracy for recovering TI-ADC output. Based on the experimental results, we found that the raw output from the TI-ADC circuits still show poor ENOB and SFDR performances. In this regard, the proposed blind

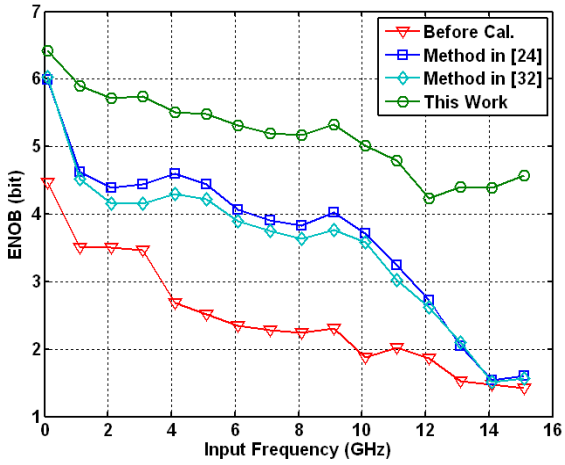

Fig. 19. ENOB performance versus input frequency.

digital calibration method is applied to compensate the residual errors, which could further improve the system performance. Fig.17 shows the measured device of the TI-ADC system, which consists of 16GHz T/H front-end board, ADC/FPGA board and display screen. These devices can be corresponding to the Fig.16. The T/H circuit net was developed by our team. The ADC was chosen from the off the shelf product (the part number is EVAQ190, E2V company). At first, we utilized the signal generator to generate a test signal and fed it to the T/H front-end network. Then the test signal was sampled by the 16-channel TI-ADC system and the processed on the FPGA board. At last, the collected samples were further compensated and displayed on the screen.

A. Experimental Results

In the experimental test, a single-tone located at 10.1 GHz carrier was sent to the TI-ADC system as input. The test result is shown in Fig.18. The spurious signals due to gain, timing skew and offset mismatches are eliminated by using the proposed calibration technique. In addition, the SNDR and SFDR were improved from 13.08 dB and 16.26 dB to 31.94 dB

and 52.41 dB. The ENOB achieved an improvement of over 3 bit.

Furthermore, a comprehensive test was implemented to measure the ENOB performance in Fig.19. It is noticed that the ENOB of this TI-ADC system decreases from 4.5 bit to 1.5 bit as the input frequency increases. The conventional methods in [24] and [32] have only achieved an improvement of 1.5 bit ENOB and degraded the same way as the input frequency increases. On the contrary, the proposed calibration technique can make an improvement of about 3 bit and behaves well when the input frequency approaches the Nyquist frequency. The ultimate result shows that the ENOB could reach 6.5 bit and 4.5 bit at low-end and high-end frequencies after blind calibration.

B. Summary and Discussion

A brief comparison among the proposed all-digital blind calibration technique and the prior state-of-the-arts is shown in Table III, to show the superiority of the proposed technique, in terms of the channel number, test signal type, and mismatch type, etc. Specifically, the proposed technique can adapt to any channel TI-ADC and calibrate the offset, gain and timing skew mismatch simultaneously in one calibration structure.

VI. Conclusion

In this paper, we have presented an all-digital blind calibration technique for any channel TI-ADC system. We have illustrated the basic theory of spurious signals due to mismatches among sub-ADCs. Based on the theory, we have developed a blind calibration structure that use the LMS algorithm to identify the mismatch coefficients and thus the spurious signals are subtracted from the sampled signal adaptively. Specifically, the proposed technique does not require a pilot input or additional reference channel. It does not need filter banks either. In addition, offset, gain and timing skew mismatches can be eliminated simultaneously. The simulations have confirmed that with the proposed calibration technique, we can achieve a considerable improvement in the SNR. The experimental results have further proved the effectiveness of the proposed calibration technique in the 16-channel TIADC system, which could lead to the ENOB improvement of $2 \sim 3$ bit.

References

[1] W. C. Black, Jr., and D. A. Hodges, "Time interleaved converter arrays," *IEEE J. Solid-State Circuits*, vol. SC-15, no. 6, pp. 1022–1029, Dec. 1980.

[2] D. Stepanovic and B. Nikolic, "A 2.8 GS/s 44.6 mW time-interleaved ADC achieving 50.9 dB SNDR and 3 dB effective resolution bandwidth of 1.5 GHz in 65 nm CMOS," *IEEE J. Solid-State Circuits*, vol. 48, no. 4, pp. 971–982, Apr. 2013.

[3] K. Doris, E. Janssen, C. Nani, A. Zanikopoulos, and G. Van der Weide, "A 480 mW 2.6 GS/s 10 b 65 nm CMOS time-interleaved ADC with 48.5 dB SNDR up to Nyquist," in *Proc. IEEE ISSCC*, Feb. 2011, pp. 180–182.

[4] M. El-Chammas *et al.*, "A 12 bit 1.6 GS/s BiCMOS 2×2 hierarchical time-interleaved pipeline ADC," *IEEE J. Solid-State Circuits*, vol. 49, no. 9, pp. 1876–1885, Sep. 2014.

[5] B. Murmann. (2013). *ADC Performance Survey 1997–2013*. [Online]. Available: https://web.stanford.edu/~murmann/adcsurvey.html

[6] Y. Liu, D. Chen, G. Zhang, N. Du, and Y. Qiu, "A 32 GS/s 8-bit time-interleaved ADC system with 16 GHz wideband RF front-end and embedded fully-blind digital calibration," in *Proc. 10th Global Symp. Millim.-Waves*, Hong Kong, 2017, pp. 140–142.

[7] B. Razavi, "Design considerations for interleaved ADCs," *IEEE J. Solid-State Circuits*, vol. 48, no. 8, pp. 1806–1817, Aug. 2013.

[8] N. Kurosawa, H. Kobayashi, K. Maruyama, H. Sugawara, and K. Kobayashi, "Explicit analysis of channel mismatch effects in time-interleaved ADC systems," *IEEE Trans. Circuits Syst. I, Fundam. Theory Appl.*, vol. 48, no. 3, pp. 261–271, Mar. 2001.

[9] S. Singh, L. Anttila, M. Epp, W. Schlecker, and M. Valkama, "Frequency response mismatches in 4-channel time-interleaved ADCs: Analysis, blind identification, and correction," *IEEE Trans. Circuits Syst. I, Reg. Papers*, vol. 62, no. 9, pp. 2268–2279, Sep. 2015.

[10] C.-C. Huang, C.-Y. Wang, and J.-T. Wu, "A CMOS 6-bit 16-GS/s time-interleaved ADC using digital background calibration techniques," *IEEE J. Solid-State Circuits*, vol. 46, no. 4, pp. 848–858, Apr. 2011.

[11] M. El-Chammas and B. Murmann, "A 12-GS/s 81-mW 5-bit time-interleaved flash ADC with background timing skew calibration," *IEEE J. Solid-State Circuits*, vol. 46, no. 4, pp. 838–847, Apr. 2011.

[12] J. Elbornsson, F. Gustafsson, and J.-E. Eklund, "Blind equalization of time errors in a time-interleaved ADC system," *IEEE Trans. Signal Process.*, vol. 53, no. 4, pp. 1413–1424, Apr. 2005.

[13] C. H. Law, P. J. Hurst, and S. H. Lewis, "A four-channel time-interleaved ADC with digital calibration of interchannel timing and memory errors," *IEEE J. Solid-State Circuits*, vol. 45, no. 10, pp. 2091–2103, Oct. 2010.

[14] S. Saleem and C. Vogel, "Adaptive blind background calibration of polynomial-represented frequency response mismatches in a two-channel time-interleaved ADC," *IEEE Trans. Circuits Syst. I, Reg. Papers*, vol. 58, no. 6, pp. 1300–1310, Jun. 2011.

[15] M. Seo, M. J. W. Rodwell, and U. Madhow, "Blind correction of gain and timing mismatches for a two-channel time-interleaved analog-to-digital converter," in *Proc. 39th IEEE Asilomar Conf. Signals, Syst., Comput.*, Oct./Nov. 2005, pp. 1121–1125.

[16] M. Seo, M. J. W. Rodwell, and U. Madhow, "Blind correction of gain and timing mismatches for a two-channel time-interleaved analog-to-digital converter: Experimental verification," in *Proc. IEEE Int. Symp. Circuits Syst. (ISCAS)*, May 2006, pp. 3394–3397.

[17] E. Venosa, F. J. Harris, and F. A. N. Palmieri, *Software Radio: Sampling Rate Selection, Design and Synchronization*. New York, NY, USA: Springer-Verlag, 2012.

[18] P. Satarzadeh, B. C. Levy, and P. J. Hurst, "Adaptive semiblind calibration of bandwidth mismatch for two-channel time-interleaved ADCs," *IEEE Trans. Circuits Syst. I, Reg. Papers*, vol. 56, no. 9, pp. 2075–2088, Sep. 2009.

[19] T. H. Tsai, P. J. Hurst, and S. H. Lewis, "Correction of mismatches in a time-interleaved analog-to-digital converter in an adaptively equalized digital communication receiver," *IEEE Trans. Circuits Syst. I, Reg. Papers*, vol. 56, no. 2, pp. 307–319, Feb. 2009.

[20] S. M. Jamal, D. Fu, N. C.-J. Chang, P. J. Hurst, and S. H. Lewis, "A 10-b 120-Msample/s time-interleaved analog-to-digital converter with digital background calibration," *IEEE J. Solid-State Circuits*, vol. 37, no. 12, pp. 1618–1627, Dec. 2002.

[21] A. Bonnetat, J.-M. Hodé, G. Ferré, and D. Dallet, "An adaptive all-digital blind compensation of dual-TIADC frequency-response mismatch based on complex signal correlations," *IEEE Trans. Circuits Syst. II, Exp. Briefs*, vol. 62, no. 9, pp. 821–825, Sep. 2015.

[22] S. J. Liu, P. P. Qi, J. S. Wang, M. H. Zhang, and W. S. Jiang, "Adaptive calibration of channel mismatches in time-interleaved ADCs based on equivalent signal recombination," *IEEE Trans. Instrum. Meas.*, vol. 63, no. 2, pp. 277–286, Feb. 2014.

[23] A. Bonnetat, J.-M. Hodé, G. Ferré, and D. Dallet, "Correlation-based frequency-response mismatch compensation of quad-TIADC using real samples," *IEEE Trans. Circuits Syst. II, Exp. Briefs*, vol. 62, no. 8, pp. 746–750, Aug. 2015.

[24] J. Matsuno, T. Yamaji, M. Furuta, and T. Itakura, "All-digital background calibration technique for time-interleaved ADC using pseudo aliasing signal," *IEEE Trans. Circuits Syst. I, Reg. Papers*, vol. 60, no. 5, pp. 1113–1121, May 2013.

[25] H. Le Duc *et al.*, "All-digital calibration of timing skews for TIADCs using the polyphase decomposition," *IEEE Trans. Circuits Syst. II, Exp. Briefs*, vol. 63, no. 1, pp. 99–103, Jan. 2016.

[26] C. Vogel, "The impact of combined channel mismatch effects in time-interleaved ADCs," *IEEE Trans. Instrum. Meas.*, vol. 54, no. 1, pp. 415–427, Feb. 2005.

[27] G. Leger, E. J. Peralias, A. Rueda, and J. L. Huertas, "Impact of random channel mismatch on the SNR and SFDR of time-interleaved ADCs," *IEEE Trans. Circuits Syst. I, Reg. Papers*, vol. 51, no. 1, pp. 140–150, Jan. 2004.
[28] M. El-Chammas and B. Murmann, "General analysis on the impact of phase-skew in time-interleaved ADCs," *IEEE Trans. Circuits Syst. I, Reg. Papers*, vol. 56, no. 5, pp. 902–910, May 2009.
[29] D. Fu, K. C. Dyer, S. H. Lewis, and P. J. Hurst, "A digital background calibration technique for time-interleaved analog-to-digital converters," *IEEE J. Solid-State Circuits*, vol. 33, no. 12, pp. 1904–1911, Dec. 1998.
[30] S. M. Jamal, D. Fu, M. P. Singh, P. J. Hurst, and S. H. Lewis, "Calibration of sample-time error in a two-channel time-interleaved analog-to-digital converter," *IEEE Trans. Circuits Syst. I, Reg. Papers*, vol. 51, no. 1, pp. 130–139, Jan. 2004.
[31] S. Huang and B. C. Levy, "Blind calibration of timing offsets for four-channel time-interleaved ADCs," *IEEE Trans. Circuits Syst. I, Reg. Papers*, vol. 54, no. 4, pp. 863–876, Apr. 2007.
[32] H. Le Duc *et al.*, "Hardware implementation of all digital calibration for undersampling TIADCs," in *Proc. IEEE Int. Symp. Circuits Syst. (ISCAS)*, May 2015, pp. 2181–2184.
[33] C. Vogel, S. Saleem, and S. Mendel, "Adaptive blind compensation of gain and timing mismatches in M-channel time-interleaved ADCs," in *Proc. 15th IEEE Int. Conf. Electron., Circuits Syst. (ICECS)*, Aug./Sep. 2008, pp. 49–52.
[34] A. S. Tehrani, H. Cao, T. Eriksson, M. Isaksson, and C. Fager, "A comparative analysis of the complexity/accuracy tradeoff in power amplifier behavioral models," *IEEE Trans. Microw. Theory Techn.*, vol. 58, no. 6, pp. 1510–1520, Jun. 2010.

Yongtao Qiu received the B.S. degree in engineering physics from Tsinghua University, Beijing, China, in 2014, where he is currently pursuing the Ph.D. degree in engineering physics.

He has been with the Institute of Electronic Engineering, China Academy of Engineering Physics since 2016. His research interests include the area of high sampling system, mainly focusing on the circuit structure and the digital background calibration techniques of the TI-ADC system.

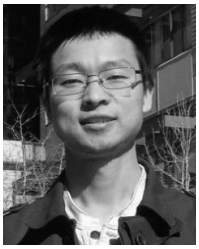

You-Jiang Liu (M'14) received the B.S. and Ph.D. degrees in engineering physics from Tsinghua University, Beijing, China, in 2008 and 2013, respectively. From 2011 to 2012, he was a Visiting Student with the Intelligent RF Radio Laboratory, Department of Electrical and Computer Engineering, University of Calgary, Calgary, AB, Canada. From 2013 to 2015, he was a Post-Doctor with High Speed Device Group, Department of Electrical and Computer Engineering, University of California, San Diego, La Jolla, CA, USA.

He has been with the Institute of Electronic Engineering, China Academy of Engineering Physics since 2015, leading an innovative research group. His research interests include signal generation, processing, and circuit design for advanced RF front-ends, e.g., digital predistortion, receive band noise cancellation, and time-interleaved analog-to-digital converter calibration.

Dr. Liu has authored/co-authored about 40 journal and conference papers. He serves as a reviewer for the IEEE TRANSACTIONS ON MICROWAVE THEORY AND TECHNIQUES, the IEEE TRANSACTIONS ON SIGNAL PROCESSING, the IEEE TRANSACTIONS ON VEHICULAR TECHNOLOGY, the IEEE TRANSACTIONS ON BROADCASTING, and the IEEE MICROWAVE AND WIRELESS COMPONENTS LETTERS.

Jie Zhou received the B.S. degree from Sichuan University, Chengdu, China, in 1995, and the M.S. degree from the Graduate School of the China Academy of Engineering Physics (CAEP), Mianyang, China, in 2001.

He is currently with the Institute of Electronic Engineering, CAEP, as a Senior Researcher. His main research interests include wireless communications and tracking telemetry command and communication.

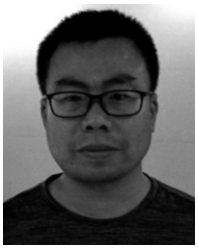

Guifu Zhang received the B.S. degree in applied physics from Hunan University, Changsha, China, in 1999, and the master's degree from the China Academy of Engineering Physics in 2004, where he is currently pursuing the Ph.D. degree in engineering physics.

He has been with the Institute of Electronic Engineering, China Academy of Engineering Physics since 2004. His research interests include the area of high sampling system, mainly focusing on the analog circuits and the sampling system construction.

Dahai Chen received the B.E., M.E., and D.E. degrees in electronic engineering from the University of Electronic Science and Technology in Chengdu, China, in 1993, 2000, and 2008, respectively.

He has been with the Institute of Electronic Engineering, China Academy of Engineering Physics since 1993. His main research interests include the area of high data rate transmission systems design and implementation.

Niantong Du received the B.S and M.S degrees in MEMS and instrument science from the Department of Precision Instrument, Tsinghua University, Beijing, China, in 2012 and 2015, respectively.

He has been with the Institute of Electronic engineering, China Academy of Engineering Physics since 2015. His main research interests include the area of digital signal processing and communication.